A computer simulation study of OH defects in Mg_2SiO_4 and Mg_2GeO_4 spinels

M. Blanchard[1], K. Wright[1,2,3], J.D. Gale[3]

[1] Royal Institution of Great Britain, 21 Albemarle Street, London W1S 4BS, UK

[2] Departments of Chemistry and Earth Sciences, University College London, Gower street, London WC1E 6BT, UK

[3] Nanochemistry Research Institute, Department of Applied Chemistry, Curtin University of Technology, P.O. Box U1987, Perth 6845, Western Australia

Communicating Author: Marc Blanchard

e-mail: marc@ri.ac.uk

Tel.: +44 (0)20 7409 2992

Fax: +44 (0)20 7629 3569

Abstract

Classical atomistic simulation techniques have been used to investigate the energies of hydrogen defects in Mg_2SiO_4 and Mg_2GeO_4 spinels. Ringwoodite (γ-Mg_2SiO_4) is considered to be the most abundant mineral in the lower part of the transition zone and can incorporate large amounts of water in form of hydroxyls, whereas the germanate spinel (γ-Mg_2GeO_4) corresponds to a low-pressure structural analogue for ringwoodite. The calculated defect energies indicate that the most favourable mechanisms for hydrogen incorporation are coupled either with the reduction of ferric iron or with the creation of tetrahedral vacancies. The hydrogen will go preferentially into tetrahedral vacancies, eventually leading to the formation of the hydrogarnet defect, before associating with other negatively charged point defects. The presence of isolated hydroxyls is not expected. The same trend is observed for germanate, and thus γ-Mg_2GeO_4 could be used as a low-pressure analogue for ringwoodite in studies of water-related defects and their effect on physical properties.

Keywords: ringwoodite, Mg_2SiO_4 spinel, Mg_2GeO_4 spinel, hydrogen, GULP.

Introduction

Since the beginning of the seventies, it has been known that nominally anhydrous mantle minerals are able to incorporate small amounts of hydrogen as point defects within their crystal structure (Martin & Donnay, 1972). The presence of this hydrogen is an important part of the process of recycling water into the Earth's interior (Bell & Rossman, 1992). It also influences the physical and chemical properties of the host phases (e.g. conductivity, viscosity, and diffusion) and thus the mantle dynamics (e.g. Kleppe et al., 2002a; Smyth et al., 2003; Jacobsen et al., 2004 for ringwoodite). The experimental study of defects in minerals is difficult and often complicated by the need to acquire data at high pressure and temperature. Computer modelling techniques have been employed to investigate defects and defect processes in minerals for over two decades and thus have an important role to play in studying the mechanisms of hydrogen uptake in mantle minerals. These methods can be used to determine the nature and the location of the H-defects in the minerals' structure as well as their vibrational properties.

Within the Earth's upper mantle and transition zone, Mg_2SiO_4 polymorphs represent the dominant minerals. The α and β phases of Mg_2SiO_4, forsterite and wadsleyite, have already been studied with simulations using both classical and quantum mechanical levels of theory (e.g. Wright & Catlow, 1994; Brodholt & Refson, 2000; de Leeuw & Parker, 2000; Braithwaite et al., 2003 for forsterite, Wright & Catlow, 1996; Haiber et al., 1997; Parker et al., 2004 for wadsleyite). However, very little modelling work has been carried out on ringwoodite, the high-pressure γ-polymorph. Hence, the work that we present here is focused on ringwoodite (γ-Mg_2SiO_4) and its analogue, the germanate spinel (γ-Mg_2GeO_4). Ringwoodite is considered to be the most abundant mineral in the lower part of the transition zone (520-660 km depth) and solubility studies performed at high-pressure from natural or

synthetic material, have shown that ringwoodite can incorporate a lot of water, up to 2.7 wt % H_2O, in the form of OH within its crystal structure (Kohlstedt et al., 1996; Bolfan-Casanova et al., 2000). However, the nature of hydrogen sites in ringwoodite remains unclear and the origin of the very broad band between 3800 and 2700 cm^{-1} associated with OH in the FTIR spectra of ringwoodite is not yet explained. The only clues come from site occupancy refinement from X-ray single-crystal diffraction data (Kudoh et al., 2000; Smyth et al., 2003). These studies mainly indicate the presence of octahedral vacancies and a small degree of Mg-Si disorder, difficult to quantify because of the close similarity of the X-ray scattering factors of Si^{4+} and Mg^{2+}. This would suggest that, in ringwoodite, the hydration is associated with vacancies in octahedral sites. As for the germanate spinel, it is stable at atmospheric pressure below 810°C as well as at high pressures (Dachille & Roy, 1960) and has been used as a low-pressure analogue for studying the olivine-spinel transition (Ringwood, 1975). A detailed comparison of the physical properties of both spinels with incorporation of hydrogen could tell us about the ability of the germanate spinel to be used as an analogue for ringwoodite, since experimental studies are complicated by its high-pressure stability field.

Classical atomistic simulation codes are an ideal tool with which to investigate a large number of possible defect configurations associated with the incorporation of hydrogen in spinels. The classical atomistic approach is based on the use of empirically derived interatomic potentials that describe interactions between ions in the system of interest. In our previous paper (Blanchard et al., in press), we have shown that the potential model used for forsterite and wadsleyite (Price et al., 1987) is unable to reproduce the elastic properties of ringwoodite. A new set of interatomic potentials was developed with the addition of a breathing shell model to treat the oxygen polarizability that is able to accurately describe the structure as well as the elastic properties of both Mg_2SiO_4 and Mg_2GeO_4 spinels considered here. The intrinsic defect population was investigated using the Mott-Littleton method (Mott

and Littleton, 1938) and the calculated defect formation energies suggest that the partial MgO Schottky defect is the most favourable defect in both spinels. Thus, in the intrinsic situation, an association in the equilibrium of magnesium and oxygen vacancies is expected.

In the present paper, we investigate the mechanisms of hydrogen incorporation in ringwoodite and its germanate structural analogue. A classical atomistic approach following the Mott-Littleton method has been used to calculate the defect formation energies. These energies enable us to discuss the nature of the hydrogen defects as well as the incorporation mechanisms.

Methodology

Ringwoodite and its germanate analogue have the cubic spinel structure (space group *Fd*3*m*), such that there is only one crystallographically distinct site for each element. Oxygen is close-packed with silicon or germanium in tetrahedral sites (8a) and magnesium in octahedral sites (16d). The spinel structure displays another octahedral site, i.e. 16c, which is vacant. The structure consists of two types of layer stacked alternately along the [111] direction; one made of MgO_6 octahedra and TO_4 tetrahedra (OT layer) and the other made of MgO_6 octahedra (O layer). The location of the 16c octahedral site is between two tetrahedra in the OT layer (Fig. 1). X-ray diffraction studies conducted on samples synthesised at pressures and temperatures representative of the lower part of the transition zone (Kudoh et al., 2000; Smyth et al., 2003) show that a disorder over the cation sites is likely, to the extent of a few percent.

The potential model used in this study is described in Blanchard et al. (in press) and thus we only describe explicitly the additional terms required by the addition of hydrogen to the system. The full set of potential parameters is given in Table 1. O-H bonds are described employing a Coulomb-subtracted Morse potential of the form:

$$U_r = D\left(1 - \exp\left[-\alpha\left(r - r_0\right)\right]\right)^2$$

where D corresponds to the dissociation of the molecule, r_0 is the equilibrium bond length and α, which coupled with the dissociation energy, is related to the vibrational frequency for the stretching mode. These parameters were fitted to the experimental data of Schröder et al. (1992). In a forthcoming study, Gatzemeier and Wright (in preparation) have refined the α parameter in order to better reproduce the theoretical OH stretching frequency obtained from the embedded QM/MM method in forsterite (Braithwaite et al., 2003). This refined value (i.e. 2.03 $Å^{-1}$) has been used here. We use fractional charges for the O and H in the OH^- ion, but the hydroxyl has a formal charge of -1. In addition, the short-range potentials involving these new species must be explicitly defined. The Buckingham potentials between a hydroxyl oxygen and magnesium, silicium, hydrogen or another hydroxyl oxygen, for which no breathing shell is implied, have been taken from the literature (Schröder et al., 1992, Wright and Catlow, 1994). No Buckingham potential was available for the interaction between the germanium and the hydroxyl oxygen. So we have derived this potential following the same method as Schröder et al. (1992) for Si^{4+}-$O^{1.4-}$. Starting from the potentials of Sastre and Gale (2003), the parameters were fitted to the structure of GeO_2 (quartz) by changing the formal charges to the fractional charges used. Finally, the Buckingham potential for O^{2-}-$O^{1.4-}$ has been chosen equal to the one for O^{2-}-O^{2-} because of the presence of the breathing shell for the lattice oxygens (O^2).

The defect energies were calculated using the Mott-Littleton method, as implemented within the GULP code (Gale and Rohl, 2003). The calculations employed a cluster with a

central region (R1) containing around 800 atoms (12 Å in radius), which was embedded in a larger region (R2), giving a total cluster radius of 22.5 Å. Within R1, all ions are explicitly relaxed to their equilibrium positions, while in R2, the effects are relatively weak and can be described by more approximate means. It has been checked that increasing the R1 radius beyond this limit results in a negligible change in the defect energetics.

Results

Ringwoodite

The potential model described above was used to determine the structures and energetics of a range of potential OH defect configurations. The defect energies, listed in Table 2, correspond to the minima on the potential energy surface reached by optimizing the structure from different starting configurations. The optimized defect structures were carefully examined. Their general configurations are always in agreement with the location of the charge deficit and with the local space available in the defective structure prior to hydrogen incorporation. The O-H bond distances were verified to be larger than the critical 0.9 Å value (Libowitzky, 1999) and rather measure about 1.02 Å. The optimized configuration of two potential OH defects is illustrated in Figure 2.

To determine the order in which intrinsic defect species may be protonated, we calculate the binding energies involved; i.e. the energy of bringing an isolated hydroxyl defect to a vacant site (Table 3). We have considered the binding energies between one or more isolated hydroxyl and a magnesium vacancy (Eq. 1 and 2), a silicon vacancy (Eq. 3, 4, 5 and 6) or a magnesium substituted for a silicon (Eq. 7 and 8):

$$V''_{Mg} + (OH)^{\bullet}_{O} \rightarrow \left[V_{Mg}(OH)\right]' \quad (1)$$

$$\left[V_{Mg}(OH)\right]' + (OH)_O^{\bullet} \rightarrow \left[V_{Mg}(OH)_2\right]^X \quad (2)$$

$$V_{Si}'''' + (OH)_O^{\bullet} \rightarrow \left[V_{Si}(OH)\right]''' \quad (3)$$

$$\left[V_{Si}(OH)\right]''' + (OH)_O^{\bullet} \rightarrow \left[V_{Si}(OH)_2\right]'' \quad (4)$$

$$\left[V_{Si}(OH)_2\right]'' + (OH)_O^{\bullet} \rightarrow \left[V_{Si}(OH)_3\right]' \quad (5)$$

$$\left[V_{Si}(OH)_3\right]' + (OH)_O^{\bullet} \rightarrow \left[V_{Si}(OH)_4\right]^X \quad (6)$$

$$Mg_{Si}'' + (OH)_O^{\bullet} \rightarrow \left[Mg_{Si}(OH)\right]' \quad (7)$$

$$\left[Mg_{Si}(OH)\right]' + (OH)_O^{\bullet} \rightarrow \left[Mg_{Si}(OH)_2\right]^X \quad (8)$$

Table 3 shows that all binding energies are negative, which indicates the presence of a significant driving force for the isolated OH species to combine with negatively charged defects, not only cation vacancies, but also the magnesium in tetrahedral site (substitution). For instance, the system gains around 11 eV by combining one hydroxyl with the magnesium vacancy instead of keeping them apart (Eqn. 1), and around 10 eV more by combining a second hydroxyl (Eqn. 2). Looking now at the relative values of these binding energies, we can establish the protonation order and therefore the nature of the most likely protonated defects. Thus, hydrogen will go preferentially into the silicon vacancies, if there are any, up to the formation of the neutral hydrogarnet-type defect. Then hydrogen will bind with substituted magnesium atoms before filling the magnesium vacancies. These results show a trend to form neutral defects, but this does not preclude the existence of defects such as $\left[V_{Si}(OH)_2\right]''$ or $\left[Mg_{Si}(OH)\right]'$ if charge compensation can occur through the presence within the crystal of other charged defects (e.g. $Fe_{Mg}^{\bullet}$, $V_O^{\bullet\bullet}$).

The calculated defect energies also provide information on the way that water dissolution occurs in ringwoodite. Indeed, by writing the appropriate reactions, one can obtain

reaction energies that can be compared thereby allowing us to identify the energetically favourable mechanisms. Four mechanisms of hydrogen incorporation are proposed here; the three reactions with water to generate the neutral protonated defects considered above; and the incorporation of hydrogen coupled to iron reduction. The latter mechanism has often been proposed as an efficient way to incorporate hydrogen in minerals such as olivine or pyroxenes (Skogby and Rossman, 1989; Kohlstedt and Mackwell, 1998; Hercule and Ingrin, 1999).
We first consider the incorporation of water in ringwoodite via the reduction of the ferric iron located at Mg sites. This reaction can be expressed as follow:

$$H_2O + 2\,Fe_{Mg}^{\bullet} + 2\,O_O^x \rightarrow 2\,(OH)_O^{\bullet} + 2\,Fe_{Mg}^x + \frac{1}{2}\,O_{2(g)} \qquad (9)$$

In order to obtain the reaction energy, equation 9 is decomposed into two components as shown below. The first component is a reduction reaction leading to the formation of an oxygen vacancy:

$$2\,Fe_{Mg}^{\bullet} + O_O^x \rightarrow 2\,Fe_{Mg}^x + V_O^{\bullet\bullet} + \frac{1}{2}\,O_{2(g)}$$

To get the energy of this reduction reaction, the vacancy and substitution energies must be summed with three other energy terms, which are the dissociation energy of a gas phase oxygen molecule (E_{OD}), the first and second electron affinities of oxygen (E_{A2}) and the third ionization energy of iron ($E_{Fe(I3)}$). Their values are given in Table 4, though we note the uncertainty in the second electron affinity of oxygen. Thus, this reaction yields an energy of -14.51 eV. The second component of equation 9 is the reaction of water with an oxygen vacancy to form two hydroxyls:

$$H_2O + V_O^{\bullet\bullet} + O_O^x \rightarrow 2\,(OH)_O^{\bullet}$$

The energy of the hypothetical gas-phase proton transfer (E_{PT}) must be included to determine the energy of this step, which is equal to 0.41 eV. Therefore, the total energy of the reaction 9 is -7.05 eV (expressed per hydroxyl), i.e. the addition of the two components described above.

The three other mechanisms that we investigate here correspond to the incorporation of water by formation of a magnesium vacancy, a silicon vacancy and a magnesium substituted for a silicon (Eqns. 10, 11 and 12 respectively).

$$H_2O + Mg_{Mg}^{x} + 2\,O_O^{x} \rightarrow \left[V_{Mg}\left(OH\right)_2\right]^{x} + MgO \quad (10)$$

$$2\,H_2O + Si_{Si}^{x} + 4\,O_O^{x} \rightarrow \left[V_{Si}\left(OH\right)_4\right]^{x} + SiO_2 \quad (11)$$

$$H_2O + Mg_{Mg}^{x} + Si_{Si}^{x} + 3O_O^{x} \rightarrow \left[Mg_{Si}\left(OH\right)_2\right]^{x} + V_{Mg}^{''} + V_O^{\bullet\bullet} + SiO_2 \quad (12)$$

These reactions have been broken down into elementary reactions following the same procedure as for the equation 9. The total energies corresponding to these three mechanisms are given in Table 4. These mechanisms assume that the hydroxyls are strongly bound to the point defects of interest (vacancy or substitution), an assumption validated by the binding energies obtained in this study. The results displayed in Table 4 suggest that reactions 9, 10 and 11 are exothermic, whereas the reaction involving the formation of magnesium substitution is endothermic. With large negative energies, two mechanisms seem to be extremely favourable. The first one, with an energy of -7.05 eV, corresponds to the water incorporation via iron reduction (Eqn. 9). The other favourable mechanism is the one associated with the formation of silicon vacancies (Eqn. 11), which releases an energy of -6.49 eV. On the other hand, the exclusive formation of magnesium substituted for silicon (Eqn. 12) is not expected to participate in the dissolution of water in ringwoodite.

Mg_2GeO_4 spinel

The same procedure, described above for ringwoodite, has been used for the germanate spinel. The defect formation energies calculated for the germanate spinel are close to those for ringwoodite (Table 2). However, we note that the creation of vacancies and magnesium substitutions in tetrahedral sites are 5 eV lower in energy in the germanate than in

ringwoodite. This observation can be explained by the difference of size between silicon and germanium. Indeed, the Ge^{4+} ion has a radius 32.5 % larger than the Si^{4+} ion in tetrahedral coordination. The same difference in formation energy is found for these defects once protonated (e.g. $\left[V_{Ge}(OH)\right]'''$, $\left[Mg_{Ge}(OH)_2\right]^X$).

These defect formation energies were then used to determine the binding energies between hydroxyls and cation vacancies or for a magnesium in the germanium site. The results, displayed in Table 3, suggest that the same protonation order as the one described in ringwoodite, will occur in γ-Mg_2GeO_4. Indeed, the hydrogen present within the crystal should go preferentially into the germanium vacancies before associating with the magnesium in germanium sites and, finally, to the magnesium vacancies.

Finally, the reaction energies have been calculated for the four possible mechanisms of hydrogen incorporation that we have considered so far (Eqn. 9, 10, 11 and 12). Obviously, equations 11 and 12 were rewritten considering germanium instead of silicon. The resulting energies for γ-Mg_2GeO_4 are very close to those obtained for ringwoodite (Table 4), although the relative order of these reaction energies is slightly modified. In the germanate spinel, the hydrogen incorporation mechanism associated with the formation of hydrogarnet defects (Eqn. 11) is now the most favourable by 0.19 eV relative to the reaction implying iron reduction (Eqn. 9). However, within the limits of the approximations of atomistic modelling theory, this energy difference must be regarded as somewhat marginal. The results suggest therefore that the same two mechanisms are the most energetically favourable for the dissolution of water in both spinels. These are the reduction of ferric iron and the creation of hydrogarnet defects.

Discussion

Our results in the previous section suggest that, for the same thermodynamic conditions, the mechanisms allowing hydrogen incorporation in spinels and the nature of the protonated defects will be identical. Therefore, the germanate spinel, which is stable at low pressure in contrast to ringwoodite, could be used as an analogue for ringwoodite in studies of the properties related to the presence of water.

This study has not considered the effect of pressure and temperature in order to simplify the calculations and thereby to make possible the investigation of a wide range of defects. In their study of the hydrous ringwoodite by high-pressure Raman spectroscopy, Kleppe et al. (2002a) have shown that protonation has only a minor effect on the lattice dynamics over the entire stability range of this mineral. Therefore we do not expect significant modifications of the hydrogen defect population and their related mechanisms with temperature, although the relative occurrence of intrinsic defect populations may change. Pressure is likely to be more influential though.

The results presented here indicate that the hydrogen incorporation mechanisms and the hydrogen defects will be the same in ringwoodite and germanate and thus we will only discuss ringwoodite, which has been the subject of several experimental studies.

Mechanisms of hydrogen incorporation

The two most energetically favourable mechanisms out of the four proposed for incorporation of hydrogen into ringwoodite are the iron reduction and the creation of silicon vacancies (Eqn. 9 and 11, respectively).

The incorporation of hydrogen is charge balanced by the iron reduction, which obviously requires the presence of iron in ringwoodite. It is generally accepted that natural ringwoodite contains about 10% of iron (i.e. Fe/(Mg+Fe)) and the determination by Mössbauer

spectroscopy of the ferric iron ratio gives $Fe^{3+}/\sum Fe = 0.15 \pm 0.004$ (O'Neill et al., 1993; McCammon et al., 2004). Hence, this redox reaction could easily occur in the mantle and for this reason, has already been proposed for the hydrogen extraction/incorporation in several mantle phases including diopside (Skogby and Rossman, 1989; Hercule and Ingrin, 1999), olivine (Kohlstedt and Mackwell, 1998) and amphiboles (Clowe et al., 1988; Dyar et al., 1993). That iron influences protonation in ringwoodite is undeniable (Kleppe et al., 2002a, 2002b; McCammon et al., 2004), but its actual role remains unclear. McCammon et al. (2004) suggest that the protonation is coupled to the incorporation of ferric iron, although there is no clear correlation between them. This would be contrary to the redox reaction written in equation 9 or would require a more complex model with several mechanisms in competition in order to explain the observations. Clearly, additional Mössbauer measurements are required to confirm the relationship between hydrogen and ferric iron.

The other energetically favourable mechanism is the one where hydrogen incorporation is associated with the creation of silicon vacancies (Eqn. 11). This result is interesting in its own right because it suggests that the incorporation of water facilitates the formation of silicon vacancies - an idea that has been suggested in the case of forsterite (Brodholt and Refson, 2000) where it has implications for silicon diffusion and hydrolytic weakening. Indeed, if we consider first the dry reactions leading to the creation of magnesium and silicon vacancies, which can be written as follows:

$$Mg_{Mg}^{x} + O_{O}^{x} \rightarrow V_{Mg}^{''} + V_{O}^{\bullet\bullet} + MgO$$

$$Si_{Si}^{x} + 2\,O_{O}^{x} \rightarrow V_{Si}^{''''} + 2V_{O}^{\bullet\bullet} + SiO_2$$

The corresponding energies are 14.13 and 36.45 eV for the formation of the MgO and SiO_2 Schottky defects respectively (Blanchard et al., in press). This energy difference is not due to the additional oxygen vacancy contained in the SiO_2 Schottky defect, but rather suggests that more intrinsic magnesium vacancies will be present in dry ringwoodite; even if their creation

remains difficult because of the large energy barrier. The corresponding hydrous case is described by equations 10 and 11, respectively, for which the reaction energies are now equal to -6.17 and -25.94 eV (i.e. values of Table 4 multiplied by the number of hydroxyls involved). We can note first that the energies required to create cation vacancies are much lower in hydrous conditions and the reactions become exothermic. This change is mainly due to the neutralisation of the unfavourable charged vacancies by hydroxyls. Secondly, the relative order of the energies is changed. The latter point is important because it suggests that silicon vacancies are now more easily created than magnesium vacancies. Thus, our calculations predict that the presence of water could dramatically change the point-defect population and therefore the diffusion mechanisms in ringwoodite.

The experimental studies of Kudoh et al. (2000) and Smyth et al. (2003), using X-ray single crystal diffraction, find that the dominant vacancies are on octahedral sites. Furthermore, they report that the octahedral site occupancy decreases with hydrogen content. Thus these authors conclude that the principal hydration mechanism involves octahedral (i.e. Mg) cation vacancies. If this is so, then some other mechanism must be operating that inhibits the formation of silicon vacancies and hence the hydrogarnet defect. It is possible that at high pressure, the formation of tetrahedral vacancies is inhibited and that Mg vacancies and Mg_{Si} substitutions are the dominant defects. In this case, hydrogen incorporation will be via the reaction given in equation 10. However, site occupancies are difficult to obtain unambiguously from X-ray diffraction alone and high quality neutron diffraction data are needed to completely resolve this issue.

Nature of hydrogen defects

Our calculations show an obvious trend for hydrogen to form neutral defects by binding to cation vacancies or, less likely, to charged substitutions. The binding energies suggest that

hydrogen will preferentially fill existing silicon vacancies first. This result is not isolated to ringwoodite; it has been shown from other computer modelling studies that the hydrogarnet defect (or at least the association of several hydroxyls into a silicon vacancy) is one of the most favourable defects in mantle minerals such as forsterite (Brodholt and Refson, 2000; Braithwaite et al., 2003), wadsleyite (Demouchy, 2004) and diopside (Gatzemeier and Wright, in preparation). However, as we have already stated, experimental studies show that hydrous ringwoodite contains very few tetrahedral vacancies, but rather octahedral vacancies and a magnesium-silicon disorder of about 5% (Kudoh et al., 2000; Smyth et al., 2003). Since isolated hydroxyls have been found to be energetically unlikely, if the above hypothesis is correct, then the following hydrogen defects are expected: $\left[V_{Mg}(OH)_2\right]^X$ and $\left[Mg_{Si}(OH)_2\right]^X$. The binding energies of these defects are close with a slight preference for hydrogen to combine first with the magnesium substituted for silicon (Table 3).

Infrared spectroscopy is an efficient method to characterize and quantify the hydrogen defects. The infrared spectrum of ringwoodite displays a broad absorption band in the wavenumber range of 2400 - 3800 cm^{-1} (Kohlstedt et al., 1996; Bolfan-Casanova et al., 2000; Smyth et al., 2003). Within this broad band, depending on the hydrogen content and the presence of iron, several peaks can be identified at about 3120, 3345 and 3695 cm^{-1}, all attributed to structural hydroxyls. Kudoh et al. (2000) based on the correlation between the O-O distance and OH stretching frequency of Nakamoto et al. (1955), proposed that the absorption bands at about 3120 and 3695 cm^{-1} correspond to protons located between O-O pairs of the 16c vacant octahedral site and the partially vacant 16d octahedral site, respectively. On the other hand, Smyth et al. (2003) attribute the same band near 3120 cm^{-1} to the protonation of the tetrahedral edge by using the correlation of Libowitzky (1999). In general, experimentally measured spectra are complex, and, as shown by the experimental disagreement, there are considerable difficulties in the assignment of individual bands.

We have calculated the OH stretching frequencies for all the defects considered and find that they fall in the range 3300 - 3800 cm^{-1} (Table 5). The optimized defect configurations show that for $\left[Mg_{Si}\left(OH\right)_2\right]^X$, the protons are in the 16c adjacent sites and for $\left[V_{Mg}\left(OH\right)_2\right]^X$, the protons are in the 16d octahedral vacant site (Fig. 2). However, our calculated IR frequencies are not sufficiently accurate to allow assignment of given values to particular defects. Although our model is able to reproduce the experimental interatomic distances (Table 6), the direction of the O-H bonds brings some doubts about the reliability of these defect configurations. The O-H···O bonds are bent with an angle smaller than the critical case of 150° (Libowitzky, 1999) because they are very often bifurcated or even trifurcated, which is unlikely (Fig. 2). Therefore, although we are able to identify clear trends in the relative mechanisms of hydrogen incorporation in ringwoodite, this work does not allow us to discuss the accurate location of hydrogen in these two likely defects or to use the OH frequencies for the attribution of the infrared absorption bands.

Conclusion

This classical atomistic modelling study has shown that the energetic trends for the hydrogen defects is the same for ringwoodite as for its structural analogue, γ-Mg_2GeO_4. In the ideal case investigated by this model, the most favourable mechanisms of hydrogen incorporation are those coupled with the iron reduction and the creation of tetrahedral vacancies. The results also indicate that the hydrogen once present within the crystal will go preferentially into the tetrahedral vacancies up to the formation of the hydrogarnet defect, before associating with the other negatively charged point defects. In order to resolve the issue of site occupancies and their influence on iron on hydrogen incorporation, further work is required. In the future,

we hope to calculate the IR spectra and determine hydrogen positions in ringwoodite using a quantum mechanical approach.

Acknowledgements This study was partially supported by the EU through the Human Potential Program HPRM-CT-2000-0056. KW would like to thanks the Royal Society for funding and JDG gratefully acknowledges the support of the Government of Western Australia through a Premier's Research Fellowship. We also thank EPSRC for provision of computing resources under grant no. GR/SO6233/01.

References

Bell, D.R., Rossman, G.R. (1992) Water in Earth's mantle: The role of nominally anhydrous minerals. Science, 255, 1391-1397.

Blanchard, M., Wright, K., Gale, J.D. (2005) Atomistic simulation of Mg_2SiO_4 and Mg_2GeO_4 spinels: a new model. Physics and Chemistry of Minerals, in press.

Bolfan-Casanova, N., Keppler, H., Rubie, D.C. (2000) Water partitioning between nominally anhydrous minerals in the MgO-SiO_2-H_2O system up to 24 GPa: implications for the distribution of water in the Earth's mantle. Earth Planet. Sci. Let., 182, 209-221.

Braithwaite, J.S., Wright, K., Catlow, C.R.A. (2003) A theoretical study of the energetics and IR frequencies of hydroxyl defects in forsterite. Journal of Geophysical Research, 108 (B6) art. no. 2284.

Brodholt, J.P., Refson, K. (2000) An ab initio study of hydrogen in forsterite and a possible mechanism for hydrolytic weakening. Journal of Geophysical Research, 105 (B8), 18977-18982.

Catlow CRA (1977) Oxygen incorporation in the alkaline earth fluoride. J. Phys. Chem. Solids 38, 1131-1136.

Clowe, C.A., Popp, R.K. and Fritz, S.J. (1988) Experimental investigation of the effect of oxygen fugacity on ferric ferrous ratios and unit cell parameters of four natural clinoamphiboles. American Mineralogist, 73, 487-499. Dachille, F. & Roy, R. (1960) Amer. J. Sci. 258, 225-246.

CRC Handbook of Chemistry and Physics. 61st Edition (1980-81) Weast, R.C. (ed) CRC Press Inc, Florida, USA

de Leeuw, N.H., Parker, S.C. (2000) Density functional theory calculations of proton-containing defects in forsterite. Radiation Effects and Defects in Solids, 154, 255-259.

Demouchy, S. (2004) Water in the Earth's interior: Thermodynamics and kinetics of hydrogen incorporation in olivine and wadsleyite. PhD thesis, Bayerisches Geoinstitut, Universität Bayreuth, pp. 156.

Dreele, R.B., Navrotsky, A. (1954) Refinement of the crystal structure of Mg_2GeO_4 spinel. Am. Mineral., 39, 957-975.

Dyar, M.D., Mackwell, S.J., McGuire, A.V., Cross, L.R. and Robertson, J.D. (1993) Crystal chemistry of Fe^{3+} and H^+ in mantle kaersutite: Implications for mantle metasomatism. American Mineralogist, 78, 968-979.

Gale, J.D, Rohl, A.L. (2003) The General Utility Lattice Program (GULP). Molecular Simulation, 29, 291-341.

Haiber, M., Ballone, P., Parrinello, M. (1997) Structure and dynamics of protonated Mg_2SiO_4: an ab-initio study. American Mineralogist, 82, 913-922.

Hercule S, Ingrin J (1999) Hydrogen in diopside: Diffusion, kinetics of extraction-incorporation, and solubility, Am. Mineral., 84, 1577-1587.

Jacobsen, S.D., Smyth, J.R., Spetzler, H., Holl, C.M., Frost, D.J. (2004) Sound velocities and elastic constants of iron-bearing hydrous ringwoodite. Phys. Earth Planet. Inter., 143-144, 47-56.

Kleppe, A.K., Jephcoat, A.P. and Smyth, J.R. (2002a) Raman spectroscopic study of hydrous γ-Mg_2SiO_4 to 56.5 GPa. Phys. Chem. Minerals, 29, 473-476.

Kleppe, A.K., Jephcoat, A.P., Smyth, J.R. and Frost, D.J. (2002b) On protons, iron and the high-pressure behavior of ringwoodite. Geophysical Research Letters, 29(21), 2021.

Kohlstedt, D.L., Keppler, H., Rubie, D.C. (1996) Solubility of water in the α, β and γ phases of $(Mg,Fe)_2SiO_4$. Contrib. Mineral. Petrol., 123, 345-357.

Kohlstedt DL, Mackwell SJ (1998) Diffusion of hydrogen and intrinsic point defects in olivine. Zeitschrift für Physikalische Chemie, 207, 147-162.

Kudoh, Y., Kuribayashi, T., Mizobata, H., Ohtani, E. (2000) Structure and cation disorder of hydrous ringwoodite, γ-$Mg_{1.89}Si_{0.98}H_{0.30}O_4$. Phys. Chem. Minerals, 27, 474-479.

Libowitzky, E. (1999) Correlation of O-H stretching frequencies and O-H···O hydrogen bond lengths in minerals. Monatshefte für Chemie/Chemical Monthly, 130, 1047-1059.

Martin, R.F., Donnay, G. (1972) Hydroxyl in the mantle. Am. Mineral., 57, 554-570.

McCammon, C.A., Frost, D.J., Smyth, J.R., Laustsen, H.M.S., Kawamoto, T., Ross, N.L. and Van Aken, P.A. (2004) Oxidation state of iron in hydrous mantle phases: implications for subduction and mantle oxygen fugacity, Physics of the Earth and Planetary Interiors, 143-144, 157-169.

Mott, N.F. & Littleton, M.J. (1938) Conduction in polar crystals. I. Electrolytic conduction in solid salts. Transactions Faraday Society, 34, 485.

Nakamoto K, Margoshes M and Rundle RE (1955) Stretching frequencies as a function of distances in hydrogen bonds. J. Am. Chem. Soc., 77, 6480-6486.

O'Neill, H.S.C., McCammon, C.A., Canil, D., Rubie, D.C., Ross II, C.R. and Seifert, F. (1993) Mössbauer spectroscopy of mantle transition zone phases and determination of minimum Fe^{3+} content, American Mineralogist, 78, 456-460.

Parker, S.C., Cooke, D.J., Kerisit, S., Marmier, A.S., Taylor, S.L., Taylor, S.N. (2004) From HADES to PARADISE – atomistic simulations of defects in minerals. Journal of Physics: Condensed Matter, 16, S2735-S2749.

Price, G.D., Parker, S.C., Leslie, M. (1987) The lattice dynamics and thermodynamics of the Mg_2SiO_4 polymorphs. Physics and Chemistry of Minerals, 15, 181-190.

Ringwood, A.E. (1975) Composition and petrology of the Earth's mantle. New York: Mc Graw-Hill.

Sastre, G., Gale, J.D. (2003) Derivation of an interatomic potential for germanium- and silicon-containing zeolites and its application to the study of the structures of octadecasil, ASU-7, and ASU-9 Materials, Chem. Mater., 15, 1788-1796.

Schröder, K.P., Sauer, J., Leslie, M., Catlow, C.R.A., Thomas, J.M. (1992) Bridging hydroxyl groups in zeolitic catalysts: a computer simulation study. Chem. Phys. Lett., 188, 320-325.

Skogby H, Rossman GR (1989) OH^- in pyroxenes: An experimental study of incorporation mechanisms and stability. Am. Mineral., 74, 1059-1065.

Smyth, J.R., Holl, C.M., Frost, D.J., Jacobsen, S.D., Langenhorst, F., McCammon, C.A. (2003) Structural systematics of hydrous ringwoodite and water in Earth's interior. Am Mineral., 88, 1402-1407.

Wright, K., Catlow, C.R.A. (1994) A computer simulation study of OH defects in olivine. Physics and Chemistry of Minerals, 20, 515-518.

Wright, K., Catlow, C.R.A. (1996) Calculations on the energetics of water dissolution in wadsleyite. Physics and Chemistry of Minerals, 23, 38-41.

Tables

Table 1. Parameters of the potential model used in this study. See text for explanations

Charges (a.u.)				
Ions	Core	Shell		
Mg	2.000			
Si	4.000			
Ge	4.000			
O^{2-}	0.800	-2.800		
$O^{1.4-}$	-1.426			
H	0.426			
Buckingham potential	A (eV)	ρ (Å)	C (eVÅ^6)	Cutoffs (Å)
$Mg-O^{2-}$	31.326316	0.30599	0.00000	10.0
$Mg-O^{1.4-}$	1060.5000	0.30920	0.00000	10.0
$Si-O^{2-}$	173.76200	0.14949	0.00000	12.0
$Si-O^{1.4-}$	983.55600	0.32052	10.66158	12.0
$Ge-O^{2-}$	327.41125	0.14045	0.00000	12.0
$Ge-O^{1.4-}$	1161.6339	0.32565	16.80860	12.0
$O^{2-}-O^{2-}$	$0.431x10^{-7}$	0.30000	48.28154	16.0
$O^{2-}-O^{1.4-}$	$0.431x10^{-7}$	0.30000	48.28154	16.0
$O^{1.4-}-O^{1.4-}$	22764.000	0.14900	27.88000	10.0
$H-O^{2-}$	5.5000000	0.25000	0.000000	10.0
$H-O^{1.4-}$	311.97000	0.25000	0.000000	1.3 to 10.0
Breathing shell model: (harmonic form)	K (eVÅ^{-2})		R_0 (Å)	
$O^{2-}-O^{2-}$	342.7170		1.20000	0.1
Core-shell spring constant	k (eVÅ^{-2})			
$O^{2-}-O^{2-}$	49.21432			
Morse (Coulomb-subtracted)	D (eV)	α (Å^{-1})	r_0 (Å)	
$H-O^{1.4-}$	7.052500	2.030	0.94850	1.3
Three-body potential: Stillinger-Weber	k(eVrad^{-2})	θ_0 (°)	ρ (Å)	ij ik jk
$O^{2-}-Si-O^{2-}$	69.2069	109.470	2.0 2.0	3.0 3.0 6.0
$O^{1.4-}-Si-O^{2-}$	69.2069	109.470	2.0 2.0	3.0 3.0 6.0
$O^{1.4-}-Si-O^{1.4-}$	69.2069	109.470	2.0 2.0	3.0 3.0 6.0
$O^{2-}-Ge-O^{2-}$	83.0034	109.470	2.0 2.0	3.0 3.0 6.0
$O^{1.4-}-Ge-O^{2-}$	83.0034	109.470	2.0 2.0	3.0 3.0 6.0
$O^{1.4-}-Ge-O^{1.4-}$	83.0034	109.470	2.0 2.0	3.0 3.0 6.0

Table 2. Calculated defect formation energies for ringwoodite and the germanate spinel (eV). Defects are described using the Kröger-Vink notation

Defects	γ-Mg_2SiO_4	γ-Mg_2GeO_4
$V_{Mg}^{''}$	25.90	26.86
$V_{Si}^{''''}$ or $V_{Ge}^{''''}$	117.96	113.21
$V_O^{\bullet\bullet}$	27.89	26.98
$Mg_{Si}^{''}$ or $Mg_{Ge}^{''}$	83.99	79.05
Fe_{Mg}^{X}	0.31	0.28
$Fe_{Mg}^{\bullet}$	-13.83	-14.44
$(OH)_O^{\bullet}$	19.02	19.12
$\left[V_{Mg}(OH)\right]'$	34.26	35.40
$\left[V_{Mg}(OH)_2\right]^X$	43.23	44.48
$\left[V_{Si}(OH)\right]'''$ or $\left[V_{Ge}(OH)\right]'''$	119.82	114.78
$\left[V_{Si}(OH)_2\right]''$ or $\left[V_{Ge}(OH)_2\right]''$	122.48	117.15
$\left[V_{Si}(OH)_3\right]'$ or $\left[V_{Ge}(OH)_3\right]'$	126.03	120.43
$\left[V_{Si}(OH)_4\right]^X$ or $\left[V_{Ge}(OH)_4\right]^X$	130.83	124.99
$\left[Mg_{Si}(OH)\right]'$ or $\left[Mg_{Ge}(OH)\right]'$	90.01	84.82
$\left[Mg_{Si}(OH)_2\right]^X$ or $\left[Mg_{Ge}(OH)_2\right]^X$	96.76	91.89

Table 3. Calculated defect binding energies for ringwoodite and the germanate spinel (eV). Reactions have been written for ringwoodite (see text) but are transferable to the germanate spinel by replacing Si by Ge

Reaction	γ-Mg_2SiO_4	γ-Mg_2GeO_4
1	-10.66	-10.58
2	-10.05	-10.04
3	-17.16	-17.55
4	-16.36	-16.75
5	-15.47	-15.84
6	-14.22	-14.56
7	-13.00	-13.35
8	-12.27	-12.05

Table 4. Values of the energy terms used in the reaction equations (see text) and calculated reaction energies for the incorporation of hydrogen in ringwoodite and in the germanate spinel (expressed per hydroxyl in eV). Reactions have been written for ringwoodite, but are transferable to the germanate spinel by replacing Si by Ge

Energy terms (eV)		
U_{MgO}	-39.66	
U_{SiO_2}	-137.29	
U_{GeO_2}	-131.76	
E_{PT}	-9.74[a]	
E_{OD}	5.16[b]	
E_{A2}	6.80[a]	
$E_{Fe(I3)}$	-30.65[b]	
Reaction	γ-Mg_2SiO_4	γ-Mg_2GeO_4
9	-7.05	-6.37
10	-3.08	-2.46
11	-6.49	-6.56
12	1.76	2.11

[a] From Catlow (1977)
[b] From the CRC handbook

Table 5. Calculated infrared OH stretching frequencies for ringwoodite and the germanate spinel (cm^{-1})

Defects	γ-Mg_2SiO_4	γ-Mg_2GeO_4
$(OH)_O^{\bullet}$	3641	3626
$\left[V_{Mg}(OH)\right]'$	3302	3316
$\left[V_{Mg}(OH)_2\right]^X$	3341, 3370	3356, 3392
$\left[V_{Si}(OH)\right]'''$ or $\left[V_{Ge}(OH)\right]'''$	3440	3446
$\left[V_{Si}(OH)_2\right]''$ or $\left[V_{Ge}(OH)_2\right]''$	3523, 3585	3530, 3586
$\left[V_{Si}(OH)_3\right]'$ or $\left[V_{Ge}(OH)_3\right]'$	3644, 3645, 3731	3640, 3640, 3719
$\left[V_{Si}(OH)_4\right]^X$ or $\left[V_{Ge}(OH)_4\right]^X$	3738, 3744, 3744, 3752	3712, 3739, 3739, 3844
$\left[Mg_{Si}(OH)\right]'$ or $\left[Mg_{Ge}(OH)\right]'$	3776	3796
$\left[Mg_{Si}(OH)_2\right]^X$ or $\left[Mg_{Ge}(OH)_2\right]^X$	3723, 3749	3789. 3792

Table 6. Experimental and calculated interatomic distances in ringwoodite (Å). Oxygen position corresponds to the center of the oxygen shell

	Sasaki et al. (1982)	This study
SiO_4 tetrahedron (8a)		
Si-O	1.66	1.67
O-O	2.70	2.73
MgO_6 octahedron (16d)		
Mg-O	2.07	2.06
O-O (shared edge)	3.00	2.98
O-O (unshared edge)	2.85	2.85
Vacant octahedron (16c)		
O-O (shared edge with SiO_4)	2.70	2.73
O-O (unshared edge with MgO_6)	2.85	2.85

Figures

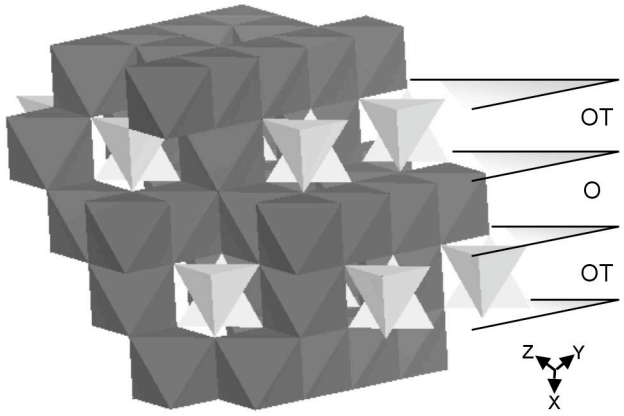

Fig. 1 Ringwoodite structure showing the alternating stacking of the OT and O layers along the [111] direction.

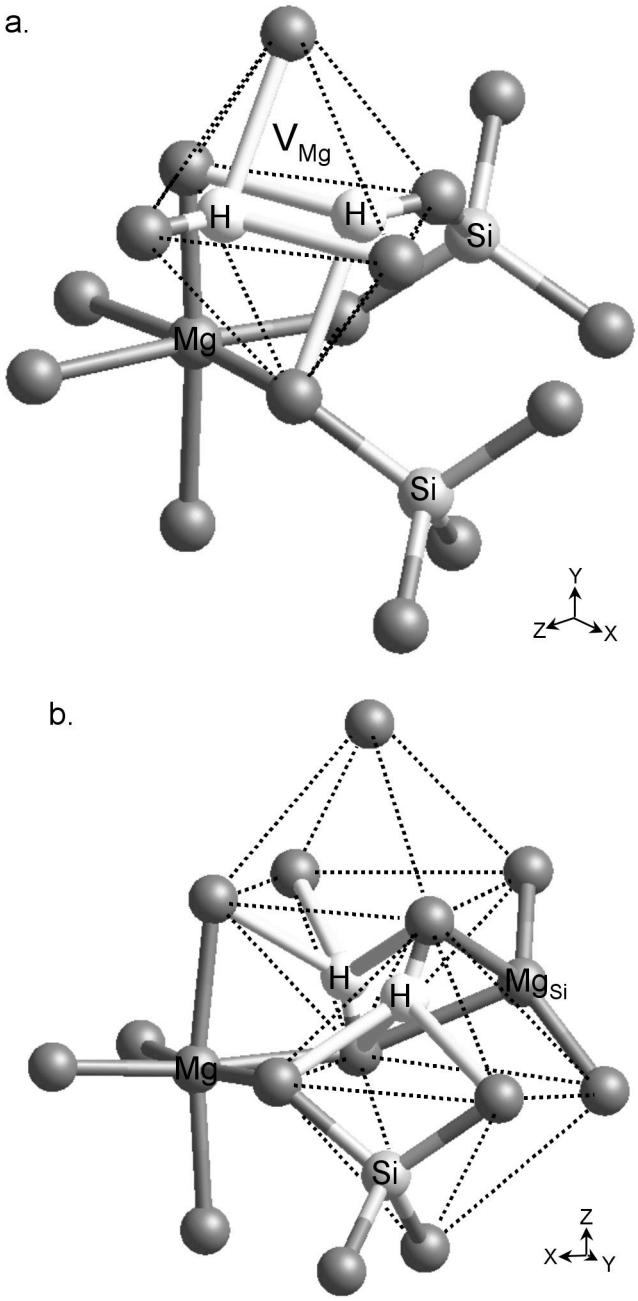

Fig. 2 a. Optimised configuration of the $\left[V_{Mg}\left(OH\right)_2\right]^X$ defect. The dashed lines highlight the magnesium vacancy (16d site). b. Optimised configuration of the $\left[Mg_{Si}\left(OH\right)_2\right]^X$ defect with the dashed lines highlighting the two 16c vacant sites adjacent to the substituted tetrahedron. In both figures, the hydrogen bonds (i.e. O-H···O) have been drawn. All unlabeled atoms are oxygen atoms.